

AEDC-TMR-85-P19



WALL INTERFERENCE EFFECTS ON ELLIPTIC MISSILE
BODY CONFIGURATIONS IN TUNNEL 4T

M. E. Sellers and T. L. Donegan
Calspan Corporation/AEDC Division

January 1986

Final Report for Period 15 September - 17 September 1985

Approved for public release; distribution is unlimited

**ARNOLD ENGINEERING DEVELOPMENT CENTER
ARNOLD AIR FORCE STATION, TENNESSEE
AIR FORCE SYSTEMS COMMAND
UNITED STATES AIR FORCE**

Report Documentation Page

*Form Approved
OMB No. 0704-0188*

Public reporting burden for the collection of information is estimated to average 1 hour per response, including the time for reviewing instructions, searching existing data sources, gathering and maintaining the data needed, and completing and reviewing the collection of information. Send comments regarding this burden estimate or any other aspect of this collection of information, including suggestions for reducing this burden, to Washington Headquarters Services, Directorate for Information Operations and Reports, 1215 Jefferson Davis Highway, Suite 1204, Arlington VA 22202-4302. Respondents should be aware that notwithstanding any other provision of law, no person shall be subject to a penalty for failing to comply with a collection of information if it does not display a currently valid OMB control number.

1. REPORT DATE JAN 1986	2. REPORT TYPE	3. DATES COVERED 15-09-1986 to 17-09-1985			
4. TITLE AND SUBTITLE Wall Interference Effects On Elliptic Missile Body Configurations In Tunnel 4T		5a. CONTRACT NUMBER			
		5b. GRANT NUMBER			
		5c. PROGRAM ELEMENT NUMBER			
6. AUTHOR(S)		5d. PROJECT NUMBER			
		5e. TASK NUMBER			
		5f. WORK UNIT NUMBER			
7. PERFORMING ORGANIZATION NAME(S) AND ADDRESS(ES) Calspan Corporation/AEDC Division,Arnold Air Force Station,TN,37389		8. PERFORMING ORGANIZATION REPORT NUMBER			
9. SPONSORING/MONITORING AGENCY NAME(S) AND ADDRESS(ES)		10. SPONSOR/MONITOR'S ACRONYM(S)			
		11. SPONSOR/MONITOR'S REPORT NUMBER(S)			
12. DISTRIBUTION/AVAILABILITY STATEMENT Approved for public release; distribution unlimited					
13. SUPPLEMENTARY NOTES					
14. ABSTRACT see report					
15. SUBJECT TERMS					
16. SECURITY CLASSIFICATION OF:			17. LIMITATION OF ABSTRACT	18. NUMBER OF PAGES	19a. NAME OF RESPONSIBLE PERSON
a. REPORT unclassified	b. ABSTRACT unclassified	c. THIS PAGE unclassified	Same as Report (SAR)	37	

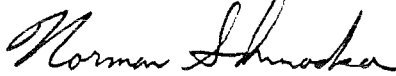
NOTICES

When U. S. Government drawings, specifications, or other data are used for any purpose other than a definitely related Government procurement operation, the Government thereby incurs no responsibility nor any obligation whatsoever, and the fact that the government may have formulated, furnished, or in any way supplied the said drawings, specifications, or other data, is not to be regarded by implication or otherwise, or in any manner licensing the holder or any other person or corporation, or conveying any rights or permission to manufacture, use, or sell any patented invention that may in any way be related thereto.

References to named commercial products in this report are not to be considered in any sense as an endorsement of the product by the United States Air Force or the Government.

APPROVAL STATEMENT

This report has been reviewed and approved.


NORMAN SCHMOEKER, 2d Lt, USAF
Aeronautical Systems Branch
Directorate of Aersp Flt Dyn Test
Deputy for Operations

Approved for publication:

FOR THE COMMANDER


ELTON R. THOMPSON
Dir, Aersp Flt Dyn Test
Deputy for Operations

REF ID: A66077

SUMMARY

Estimates of the test section wall interference effects have been computed for an elliptic missile body configuration in the Aerodynamic Wind Tunnel (4T) of the Propulsion Wind Tunnel Facility. Results are presented for test Mach numbers of 0.95 and 1.05. Comparisons of test section wall static pressure measurements in 4T with computations show relatively good agreement at Mach 0.95 and follow the general trend at Mach 1.05. The wall interference produces a 2.5% decrease in lift coefficient at the highest angle of attack for which calculations were made.

CONTENTS

	<u>Page</u>
SUMMARY	1
NOMENCLATURE	4
1.0 INTRODUCTION	5
2.0 COMPUTATIONAL MESH	5
3.0 RESULTS AND DISCUSSION	6
3.1 M = 0.95, α = 10 deg	7
3.2 M = 1.05, α = 10 deg	7
3.3 M = 0.95, α = 20 deg	7
4.0 WALL PRESSURE COMPARISONS	7
5.0 CONCLUSIONS	8
REFERENCES	8

ILLUSTRATIONS

Figure

1. Elliptic Missile Body Test Article Geometry	9
2. Computational Model Surface	10
3. Computational Mesh in Horizontal Plane	12
4. Computational Mesh in Symmetry Plane	13
5. Tunnel Surface Mesh	14
6. Distribution of Interference on Model Surface, M = 0.95, α = 10 deg.....	15
7. Distribution of Interference on Tunnel Boundary, M = 0.95, α = 10 deg.....	17
8. Symmetry Plane Contours of Pressure Differences, M = 0.95, α = 10 deg.....	19
9. Distribution of Interference on Model Surface, M = 1.05, α = 10 deg	20
10. Distribution of Interference on Tunnel Boundary, M = 1.05, α = 10 deg.....	22
11. Symmetry Plane Contours of Pressure Differences, M = 1.05, α = 10 deg	24
12. Distribution of Interference on Model Surface, M = 0.95, α = 20 deg	25
13. Distribution of Interference on Tunnel Boundary, M = 0.95, α = 20 deg	27

<u>Figure</u>	<u>Page</u>
14. Symmetry Plane Contours of Pressure Differences, M = 0.95, α = 20 deg	29
15. Computed and Measured Lift vs. Angle-of-Attack in PWT-4T, M = 0.95	30
16. Computed and Measured Wall Static Pressure Comparisons in PWT-4T	31

TABLES

<u>Table</u>	
1. Summary of Integrated Wall Interference Effects on Model Force and Moment	35

NOMENCLATURE

C_L	Lift coefficient
C_m	Pitching moment coefficient
C_p	Pressure coefficient $(p-p_\infty)/q_\infty$
IC_p	Interference pressure coefficient (C_p unconfined flow - C_p confined flow)
M	Mach number
p	Pressure, psfa
q	Dynamic pressure, psf
α	Model angle of attack, degrees
ΔC_L	Interference lift coefficient (C_L unconfined flow - C_L confined flow)
ΔC_m	Interference pitching moment coefficient (C_m unconfined flow - C_m confined flow)
ΔC_p	Wall static pipe C_p at lift coefficient of interest - wall static pipe C_p at zero lift
Subscripts	
∞	Test section reference conditions

1.0 INTRODUCTION

Wall interference produced by a tunnel upon a model is a contributor to errors inherent to measured wind tunnel data. In every transonic wind tunnel test, wall interference exists to some degree. Therefore, it is advantageous to correctly identify the level of wall interference in wind tunnel tests.

Recently an elliptic missile configuration (Fig. 1) was tested in Tunnel 4T to provide a data base for verification of computational fluid dynamics (CFD) methods. Because of the relatively large model size (1.2% blockage) and high transonic Mach numbers tested, wall interference effects were of major concern. The ARO-1 code, an Euler solver, developed at AEDC (Ref. 1) is used in this analysis to estimate the wall interference on the elliptic missile configuration. The method consists of computing the flow field about a body within a tunnel with the porous walls modelled by an empirical correlation and then computing the unconfined flow about the same body. The wall interference is the difference between the two solutions.

The calculations were made on the elliptic body at free-stream Mach numbers of 0.95 and 1.05. The angle of attack was 10 deg for both Mach numbers; a flow case of $\alpha = 20$ deg and $M_\infty = 0.95$ was also computed.

Calculations of wall interference effects on an elliptic missile body geometry, Fig. 1, was requested by Air Force Wright Aeronautical Laboratories (AFWAL/FIMG), Wright-Patterson AFB, Ohio, under Program Element 62201F, Control Number 2404. The program manager was Lt. Norman Schmoeker, AEDC/DOFA. The results were obtained by Calspan Corporation/AEDC Division, operating contractor for the aerospace flight dynamics testing effort at the AEDC, AFSC, Arnold Air Force Station, Tennessee. The analysis was conducted in the Propulsion Wind Tunnel Facility (PWT) during the period from 17 September through 20 December 1985 under AEDC project number CD48PB, PWT Test Number TC793. Documentation of the test is contained in Ref. 2.

2.0 COMPUTATIONAL MESH

The process of computing wall interference in the present methodology requires two computational meshes. One mesh models the space between the aerodynamic body and the tunnel walls to calculate the confined flow in the tunnel. This simulation is done by applying appropriate porous wall boundary conditions at the mesh outer boundary. Computational space is then added to the exterior of the first mesh resulting in the second mesh for calculations of the unconfined flow about the body. With the additional space and freestream conditions imposed on the second mesh outer boundary, unconfined flow on the body may be simulated. The difference of the two solutions is the wall interference. Two meshes are required for each angle of attack case considered because of the change in model attitude relative to the tunnel walls.

The B25 elliptic body configuration (Fig. 1) was described analytically and a computational surface grid constructed. The present method requires the body to be closed; therefore, a conical section was added to the base of the body. This addition simulates the wake region better than a flat base. Because of symmetry, only half of the tunnel and model were modelled to minimize the mesh points required. Approximately 900 mesh points were used on half the model surface.

The surface grid was transformed into a warped spherical grid topology to be used as the inner boundary of the tunnel mesh. Two views of the surface mesh are shown in Fig. 2. After analytically describing the tunnel surface, the inner model surface and outer tunnel surface were used as boundary conditions for a three-dimensional Poisson equation solver (Ref. 3) to create the interior mesh. Two planar views of the model at 10° angle of attack are shown within Tunnel 4T (Figs. 3 and 4) to demonstrate the interior mesh. Also, the model surface is shown positioned inside the tunnel surface in Fig. 5.

3.0 RESULTS AND DISCUSSION

Computations of wall interference have been made on the B25 elliptic missile body configuration in Tunnel 4T. The calculations were obtained at three flow conditions:

- 1) $M_\infty = 0.95$, $\alpha = 10$ deg
- 2) $M_\infty = 1.05$, $\alpha = 10$ deg
- 3) $M_\infty = 0.95$, $\alpha = 20$ deg

The wall porosity for all cases is 5%. The results are presented separately for each of the above cases. In each case, the wall interference is illustrated as a pressure coefficient increment produced by the wall. Therefore, the pressure contours shown in Figs. 6-14 are the differences (ICp) between the unconfined flow pressures and the tunnel confined flow pressures. In addition, the pressure differences were integrated over the body to obtain the incremental interference lift and pitching moment coefficients. These coefficients are presented in Table 1 for the three cases investigated.

As illustrated in Fig. 15, the ARO-1 code underpredicted the lift on the model; consistently lower lift curve slopes are always evident in the calculations when compared to experimental data. The measured lift coefficient data were obtained from the Elliptic Missile Body Force Test documented in Ref. 4. The mismatch occurs because viscous effects are ignored and computer storage restrictions do not allow complete resolution of the entire model. However, the results are usable if one recognizes that the increment attributable to wall interference is proportional to lift. Therefore, the comparisons with experimental data should be made with matched lift coefficients rather than angle of attack.

3.1 $M_\infty = 0.95$, $\alpha = 10$ deg

The pressure difference distribution on the elliptic body is shown in Fig. 6 for the top and bottom surfaces. The wall interference on the body is initially small near the nose but increases axially along the body. Also, the bottom surface pressure difference contours are shifted aft from the corresponding contours on the top surface illustrating the angle of attack.

The wall interference effect at the tunnel walls is shown in Fig. 7. The proximity of the base of the body to the bottom wall is evident by the high gradient and level of contours on the wall. At the tunnel symmetry plane, the patterns of pressure difference in the tunnel are shown in Fig. 8. The pressure difference contours on the base conical addition are significant, but since this addition does not exist in the actual testing of the model, these contours may be disregarded.

3.2 $M_\infty = 1.05$, $\alpha = 10$ deg

The effect of a higher free-stream Mach number is shown in this flow case. The pressure difference contours are at a lower absolute level on the body (Fig. 9) however, the interference lift coefficient is higher as shown in Table 1. The pressure difference contours are at a higher absolute level on the tunnel walls (Fig. 10) with the same basic patterns as Case 1. The interference effects at the symmetry plane (Fig. 11) are also consistent with the previous case but show a more pronounced interference pattern in the tunnel.

3.3 $M_\infty = 0.95$, $\alpha = 20$ deg

This flow case shows the effect of a higher angle of attack on the wall interference in the tunnel. As shown in Figs. 12 thru 14, the pressure difference contour levels have intensified on the body and the tunnel walls. The contour patterns have also changed on the tunnel walls since the model attitude is different. The interference is extensive as compared to the previous cases.

Considering these three flow cases, the results show that a higher free-stream Mach number causes higher levels of wall interference on the model based on interference lift coefficient. Also, higher angles of attack result in a significant increase in wall interference.

4.0 WALL PRESSURE COMPARISONS

In this section, wall pressure measurements, taken by static pressure pipes located on the centerline of the top and bottom walls, are compared to calculations on the top and bottom walls for four cases:

- 1) $M_\infty = 0.95$, $C_L = 0.6$
- 2) $M_\infty = 0.95$, $C_L = 2.1$
- 3) $M_\infty = 1.05$, $C_L = 0.6$
- 4) $M_\infty = 1.05$, $C_L = 2.1$

Because of local effects of the static pipe, wall pressure data at zero lift were subtracted from wall pressure data of each case considered and compared to calculations made similarly. These pressure differences (ΔC_p) are plotted versus tunnel station in Fig. 16.

The wall pressure comparisons at $M_\infty = 0.95$ and $C_L = 0.6$ (Fig. 16a) show good agreement on the top wall with fair prediction of the pressure trends on the bottom wall. For the higher lift case (Fig. 16b), the same trends occur on both walls. For the $M_\infty = 1.05$ cases (Figs. 16c and 16d), the data is scattered enough that no good comparison can be made. However, the calculations show a consistent trend as compared to the $M_\infty = 0.95$ cases and a general trend may be seen in the data as compared to the calculations. This data scatter may occur because of inherent problems associated with testing near $M_\infty = 1$.

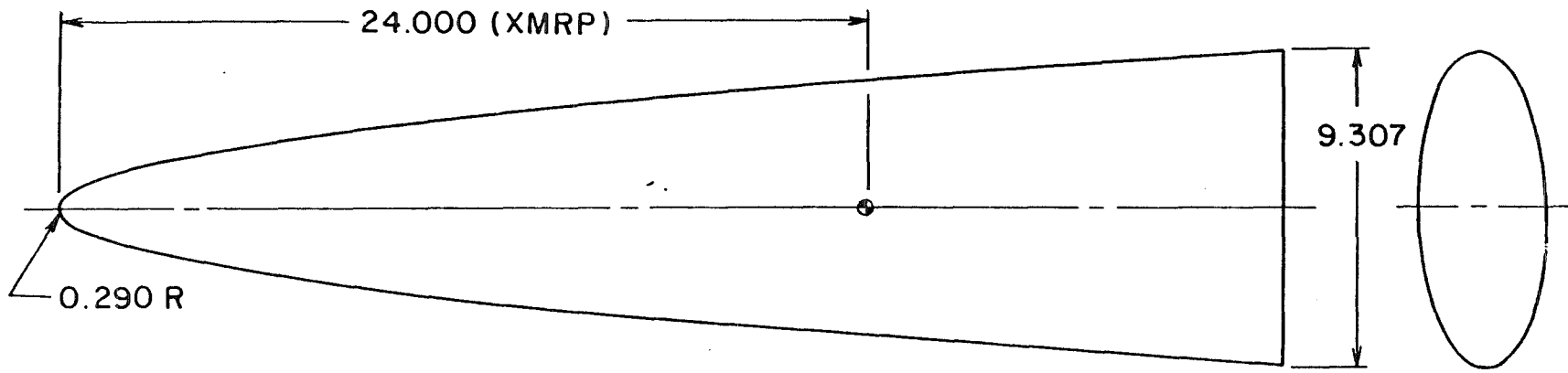
Based on previous experience, the quality of the comparisons between calculated and measured pressure coefficients near the wall is an indication that the actual wall effects on the model should be relatively close to those of the calculations.

5.0 CONCLUSIONS

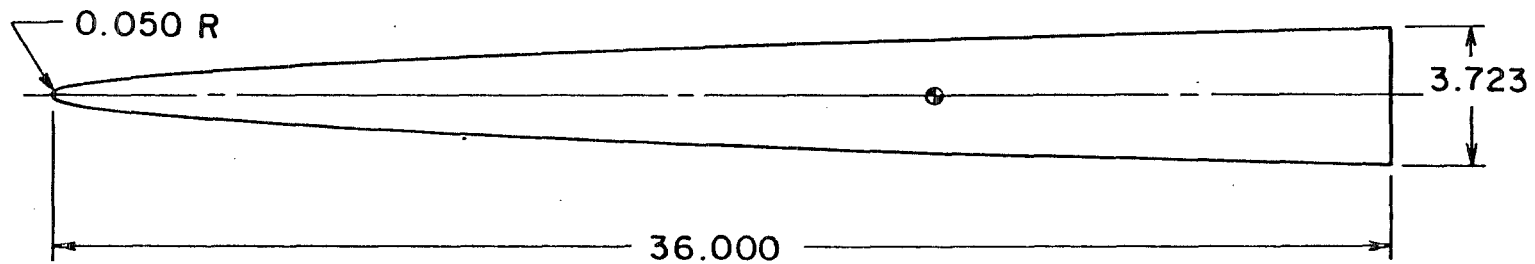
Computations of wall interference on the B25 elliptic missile configuration have been presented. Agreement between the measured and computed wall pressures provides a level of confidence that the computed interference on the body is good. The wall interference produces a 2.5% decrease in lift coefficient at the highest angle of attack for which calculations were made. These wall interference effects should be accounted for if the measured data are to be used to verify computational fluid dynamics codes.

REFERENCES

1. Farris, R. C. and Jacocks, J. L. "Prediction of Transonic Wind Tunnel Wall Interference." AEDC-TR-83-48, December 1983.
2. Sellers, M. E. "Pressure Test of Three Elliptic Missile Body Configurations." AEDC-TSR-85-P19, October 1985.
3. Shieh, C. F. "Three Dimensional Grid Generation Using Elliptic Equations with Direct Grid Distribution Control." AIAA Paper No. 83-0448, January 1983.
4. Sellers, M. E. "Static Stability Test of Three Elliptic Missile Body Configurations." AEDC-TSR-85-P8, May 1985.



TOP VIEW



SIDE VIEW

DIMENSIONS IN INCHES

B25 Configuration

Figure 1. Elliptic Missile Body Test Article Geometry



a. Top View

Figure 2. Computational Model Surface



b. Side View

Figure 2. Concluded

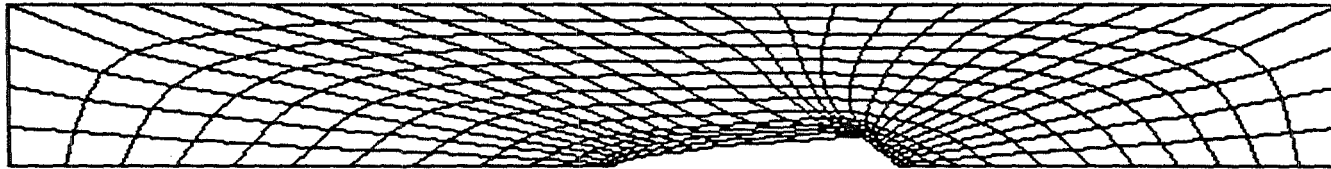


Figure 3. Computational Mesh in Horizontal Plane

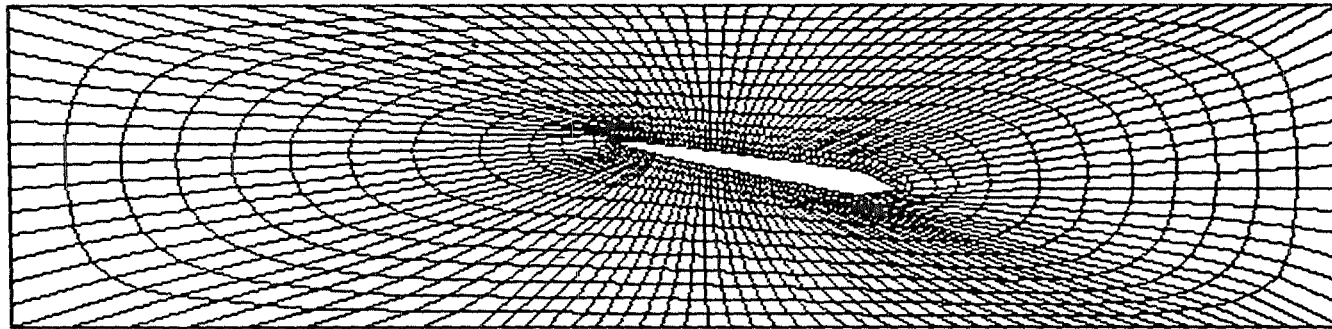


Figure 4. Computational Mesh in Symmetry Plane

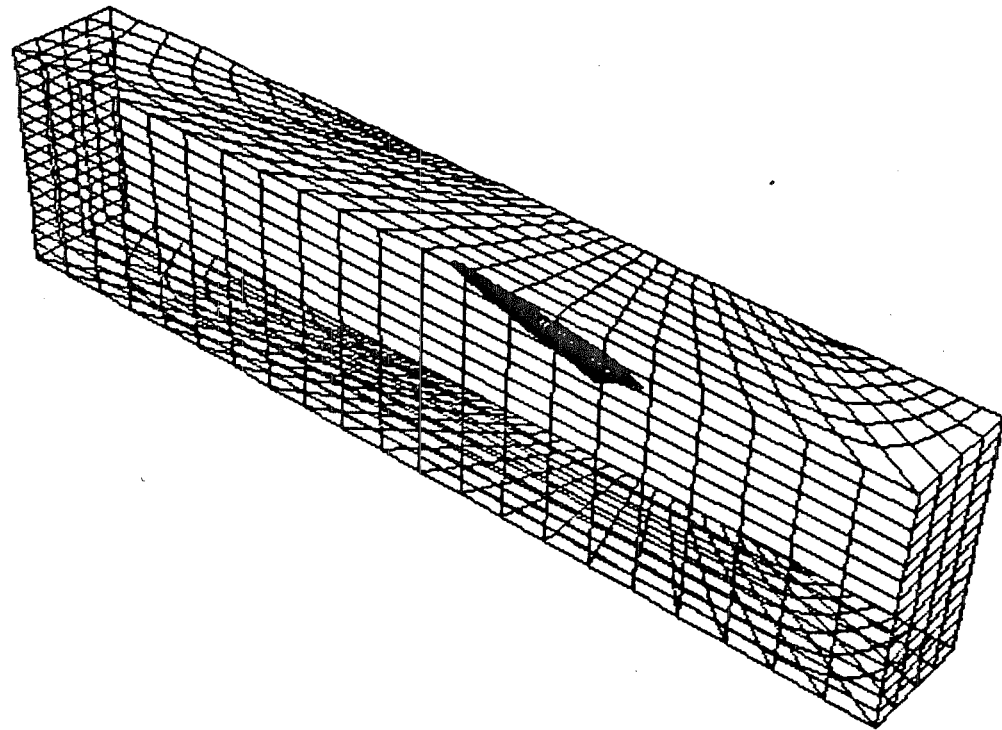


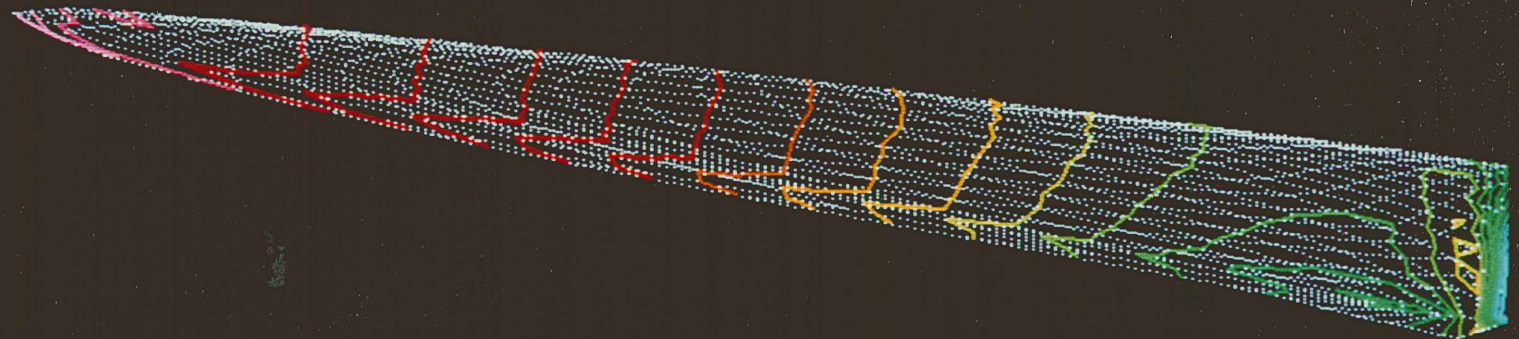
Figure 5. Tunnel Surface Mesh

PRESSURE COEFFICIENT

CONTOUR LEVELS

- .02400
- .02300
- .02200
- .02100
- .02000
- .01900
- .01800
- .01700
- .01600
- .01500
- .01400
- .01300
- .01200
- .01100
- .01000
- .00900
- .00800
- .00700
- .00600
- .00500
- .00400
- .00300
- .00200
- .00100
- 0.00000
- 0.00100
- 0.00200
- 0.00300
- 0.00400

0.950 MACH
10.00 DEG ALPHA
2.00x10⁶ Re
30x31x14 GRID



a. Top Surface

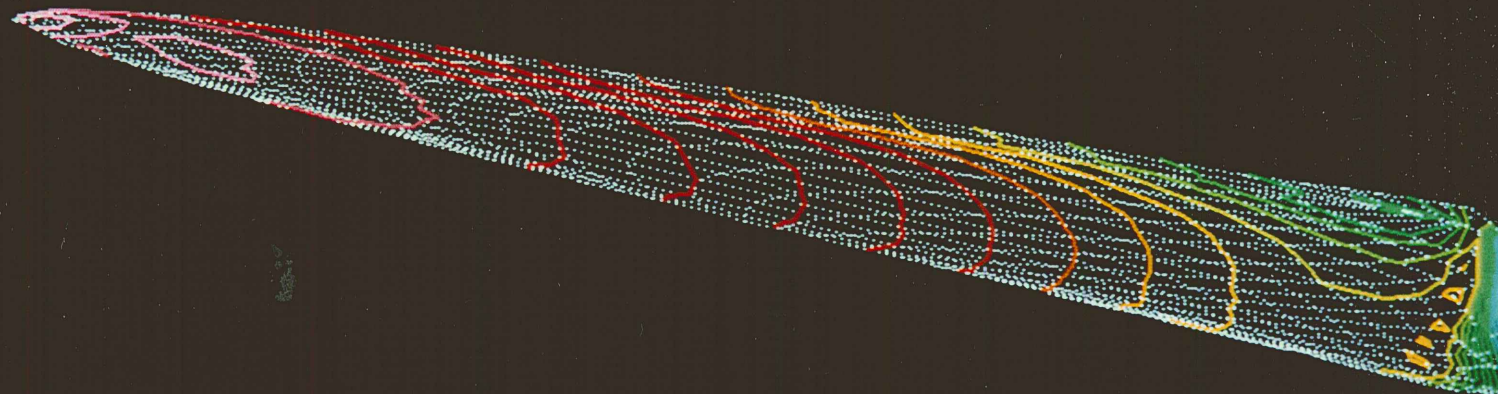
Figure 6. Distribution of Interference on Model Surface,
 $M_\infty = 0.95$, $\alpha = 10$ deg.

PRESSURE COEFFICIENT

CONTOUR LEVELS

- 0.02400
- 0.02300
- 0.02200
- 0.02100
- 0.02000
- 0.01900
- 0.01800
- 0.01700
- 0.01600
- 0.01500
- 0.01400
- 0.01300
- 0.01200
- 0.01100
- 0.01000
- 0.00900
- 0.00800
- 0.00700
- 0.00600
- 0.00500
- 0.00400
- 0.00300
- 0.00200
- 0.00100
- 0.00000
- 0.00100
- 0.00200
- 0.00300
- 0.00400

0.950 MACH
10.00 DEG ALPHA
2.00x10⁶ Re
30x31x14 GRID



b. Bottom Surface
Figure 6. Concluded.

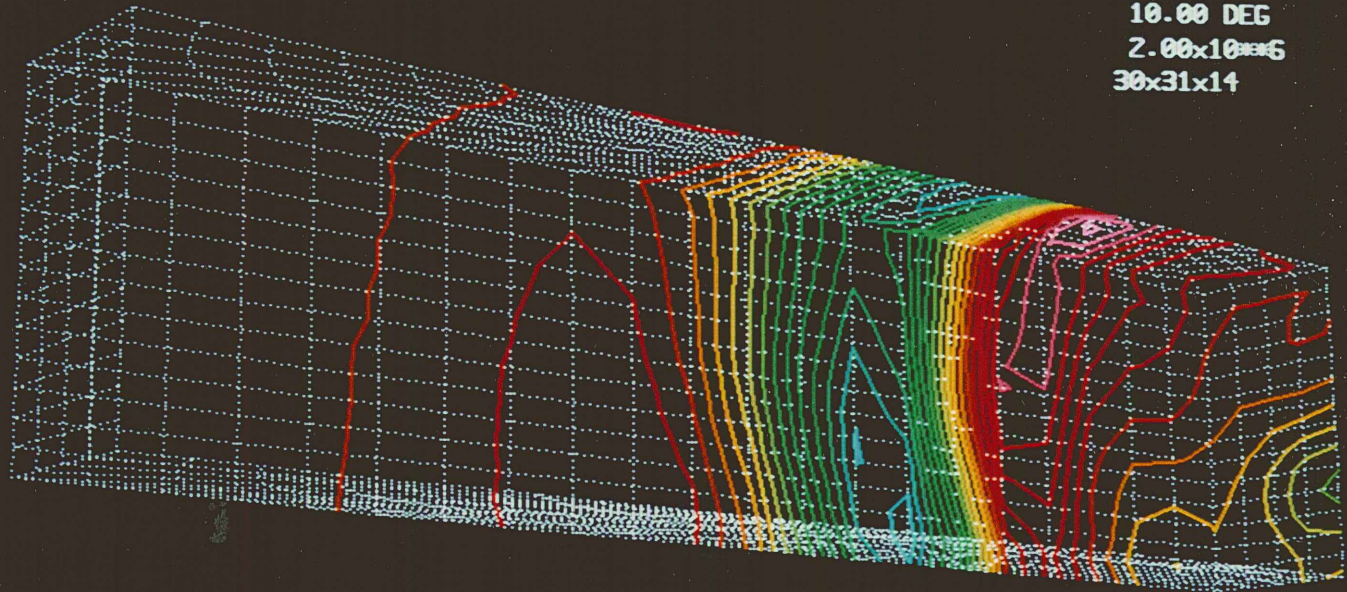
PRESSURE COEFFICIENT

CONTOUR LEVELS

- 0.01800
- 0.01700
- 0.01600
- 0.01500
- 0.01400
- 0.01300
- 0.01200
- 0.01100
- 0.01000
- 0.00900
- 0.00800
- 0.00700
- 0.00600
- 0.00500
- 0.00400
- 0.00300
- 0.00200
- 0.00100
- 0.00000
- 0.00100
- 0.00200
- 0.00300
- 0.00400
- 0.00500
- 0.00600
- 0.00700
- 0.00800
- 0.00900

0.950
10.00 DEG
2.00x10⁶
30x31x14

MACH
ALPHA
Re
GRID



a. Top and Side Surface
Figure 7. Distribution of Interference on Tunnel Boundary,
 $M_\infty = 0.95$, $\alpha = 10$ deg.

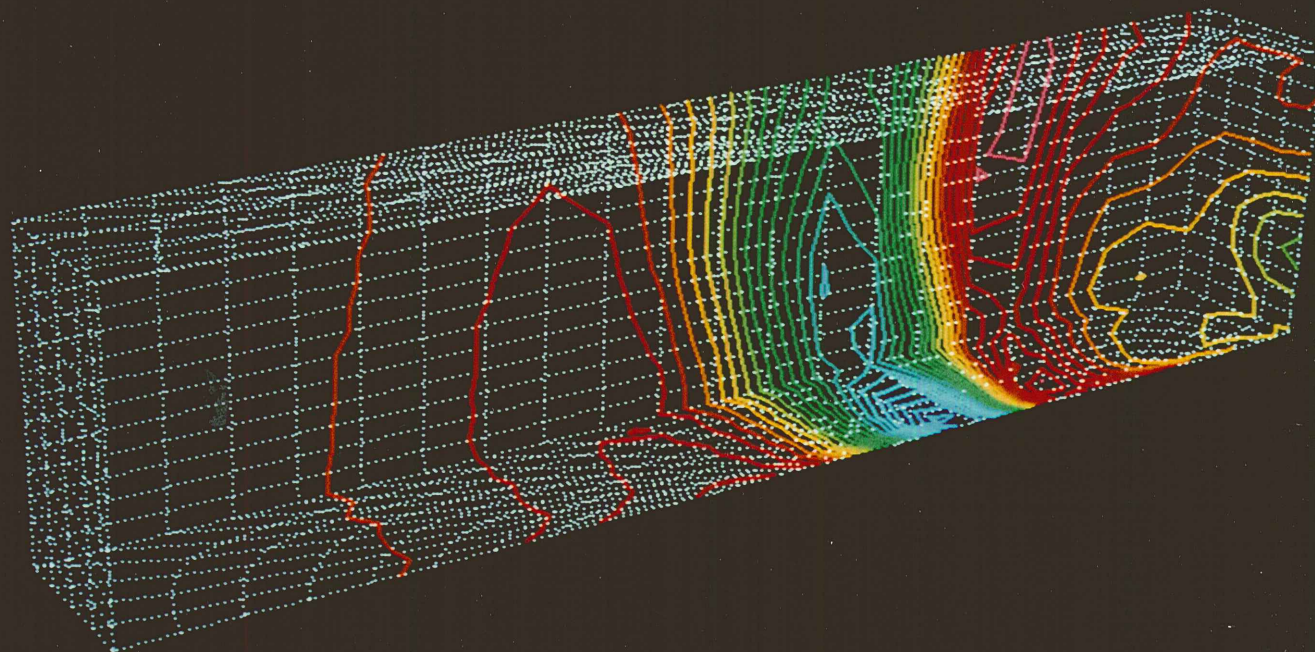
PRESSURE COEFFICIENT

CONTOUR LEVELS

- .01800
- .01700
- .01600
- .01500
- .01400
- .01300
- .01200
- .01100
- .01000
- .00900
- .00800
- .00700
- .00600
- .00500
- .00400
- .00300
- .00200
- .00100
- 0.00000
- 0.00100
- 0.00200
- 0.00300
- 0.00400
- 0.00500
- 0.00600
- 0.00700
- 0.00800
- 0.00900

0.950
10.00 DEG
2.00x10⁶
30x31x14

MACH
ALPHA
Re
GRID



b. Bottom and Side Surface
Figure 7. Concluded.

PRESSURE COEFFICIENT

CONTOUR LEVELS

- .02000
- .01800
- .01600
- .01400
- .01200
- .01000
- .00800
- .00600
- .00400
- .00200
- 0.00000
- 0.00200
- 0.00400
- 0.00600
- 0.00800

0.950
10.00 DEG
2.00x10⁶
30x31x14

MACH
ALPHA
Re
GRID

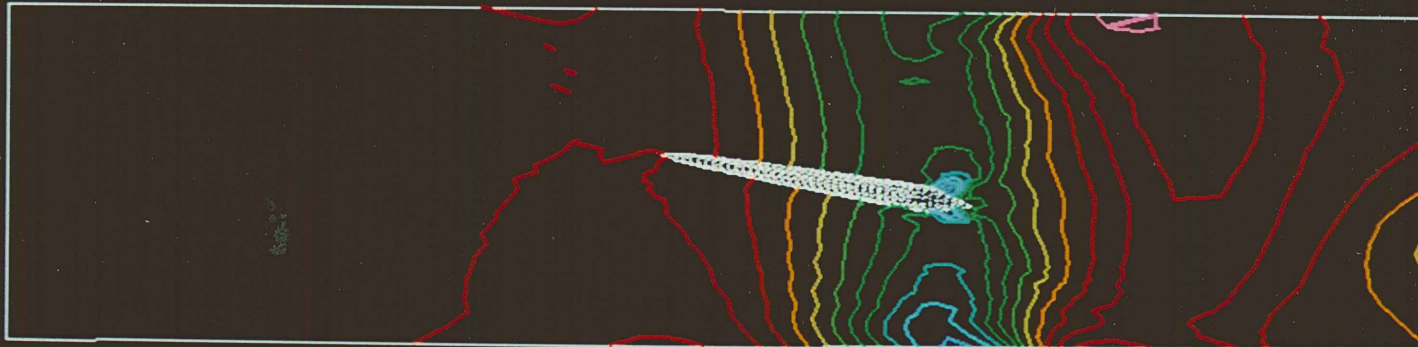


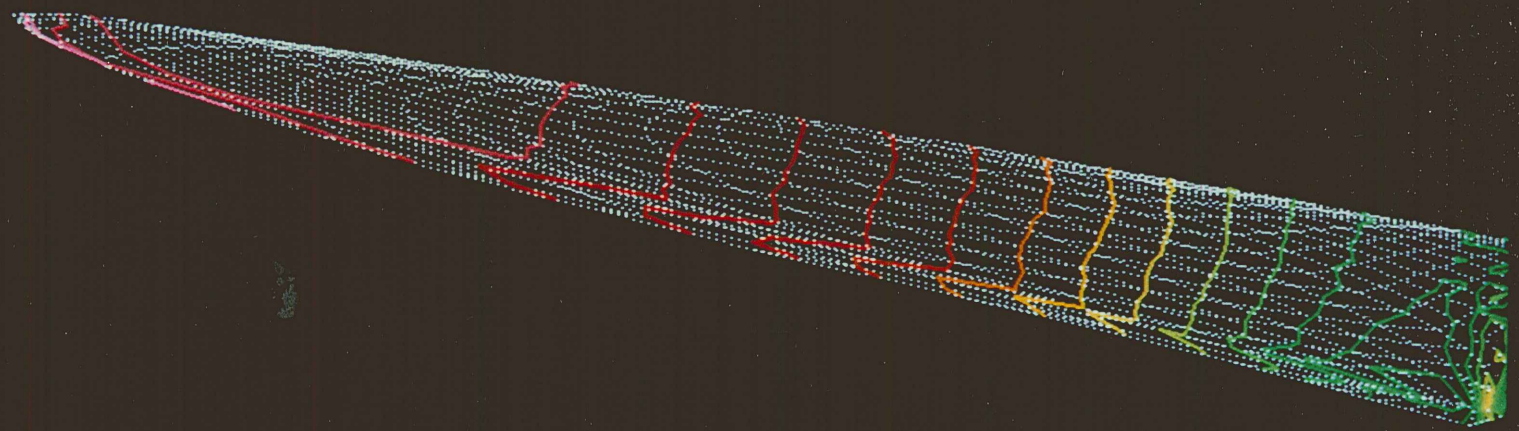
Figure 8. Symmetry Plane Contours of Pressure Differences,
 $M_\infty = 0.95$, $\alpha = 10$ deg.

PRESSURE COEFFICIENT

CONTOUR LEVELS

- .01800
- .01700
- .01600
- .01500
- .01400
- .01300
- .01200
- .01100
- .01000
- .00900
- .00800
- .00700
- .00600
- .00500
- .00400
- .00300
- .00200
- .00100
- 0.00000
- 0.00100
- 0.00200
- 0.00300
- 0.00400
- 0.00500
- 0.00600

1.050 MACH
10.00 DEG ALPHA
2.00x10⁶ Re
30x31x14 GRID



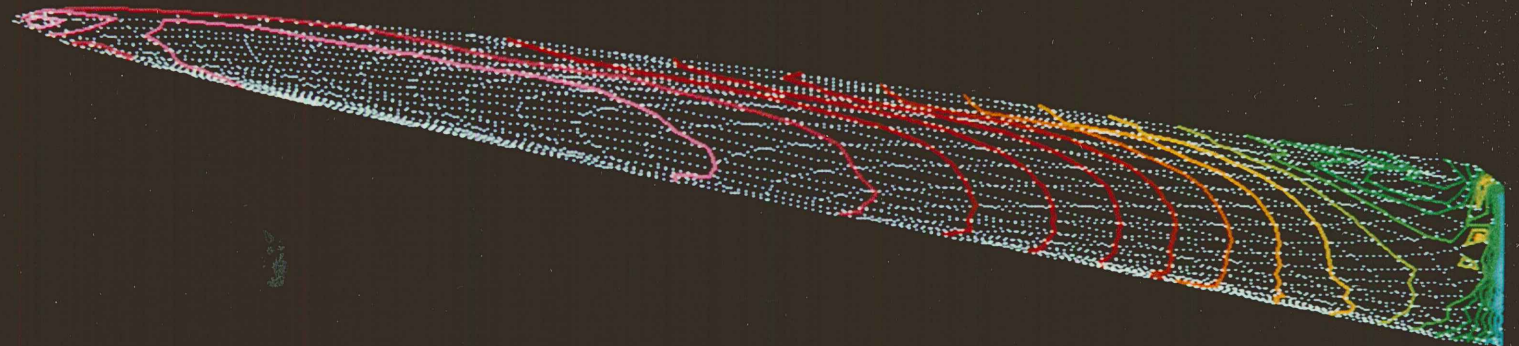
a. Top Surface
Figure 9. Distribution of Interference on Model Surface,
 $M_\infty = 1.05$, $\alpha = 10$ deg.

PRESSURE COEFFICIENT

CONTOUR LEVELS

- .01800
- .01700
- .01600
- .01500
- .01400
- .01300
- .01200
- .01100
- .01000
- .00900
- .00800
- .00700
- .00600
- .00500
- .00400
- .00300
- .00200
- .00100
- 0.00000
- 0.00100
- 0.00200
- 0.00300
- 0.00400
- 0.00500
- 0.00600

1.050 MACH
10.00 DEG ALPHA
 2.00×10^{06} Re
30x31x14 GRID



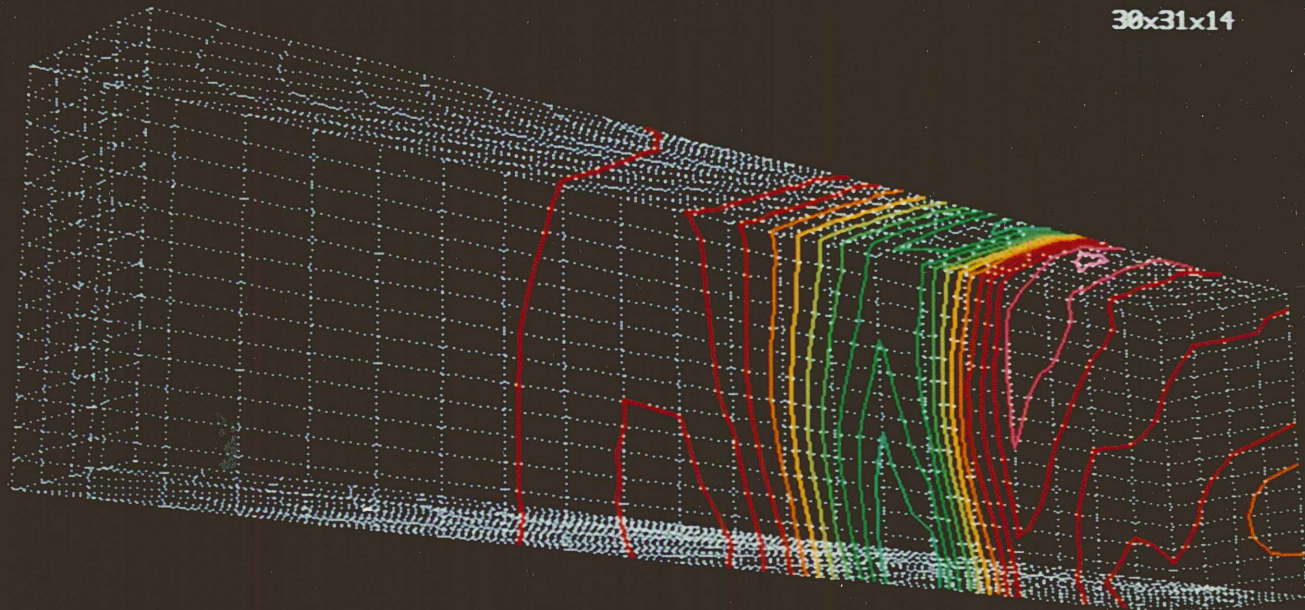
b. Bottom Surface
Figure 9. Concluded.

PRESSURE COEFFICIENT

CONTOUR LEVELS

- 0.02600
- 0.02400
- 0.02200
- 0.02000
- 0.01800
- 0.01600
- 0.01400
- 0.01200
- 0.01000
- 0.00800
- 0.00600
- 0.00400
- 0.00200
- 0.00000
- 0.00200
- 0.00400
- 0.00600
- 0.00800
- 0.01000

1.050 MACH
10.00 DEG ALPHA
2.00x10⁶ Re
30x31x14 GRID



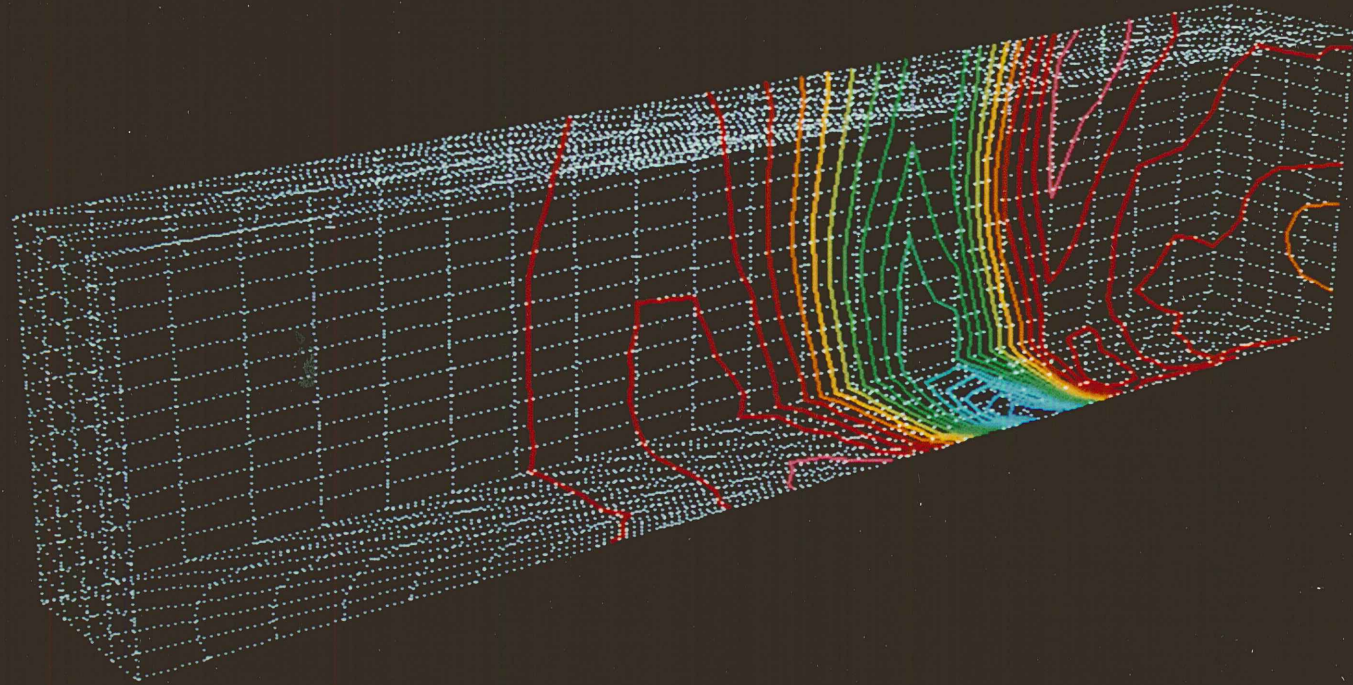
a. Top and Side Surface
Figure 10. Distribution of Interference on Tunnel Boundary,
 $M_\infty = 1.05$, $\alpha = 10$ deg.

PRESSURE COEFFICIENT

CONTOUR LEVELS

- 0.02500
- 0.02400
- 0.02200
- 0.02000
- 0.01800
- 0.01600
- 0.01400
- 0.01200
- 0.01000
- 0.00800
- 0.00600
- 0.00400
- 0.00200
- 0.00000
- 0.00200
- 0.00400
- 0.00600
- 0.00800
- 0.01000

1.050 MACH
10.00 DEG ALPHA
2.00x10⁶ Re
30x31x14 GRID



b. Bottom and Side Surface
Figure 10. Concluded.

PRESSURE COEFFICIENT

CONTOUR LEVELS

-.03200
 -.03000
 -.02800
 -.02600
 -.02400
 -.02200
 -.02000
 -.01800
 -.01600
 -.01400
 -.01200
 -.01000
 -.00800
 -.00600
 -.00400
 -.00200
 0.00000
 0.00200
 0.00400
 0.00600
 0.00800

1.050 MACH
 10.00 DEG ALPHA
 2.00×10^{06} Re
 30x31x14 GRID

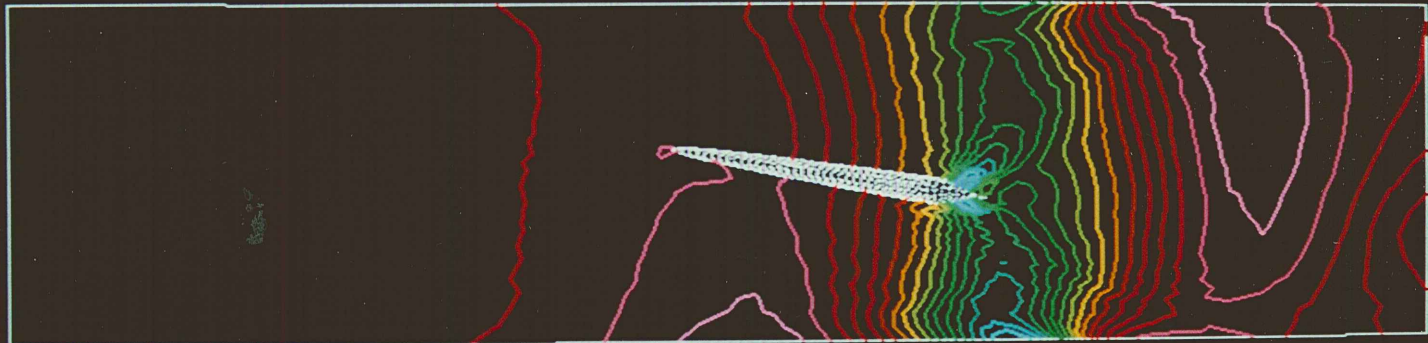


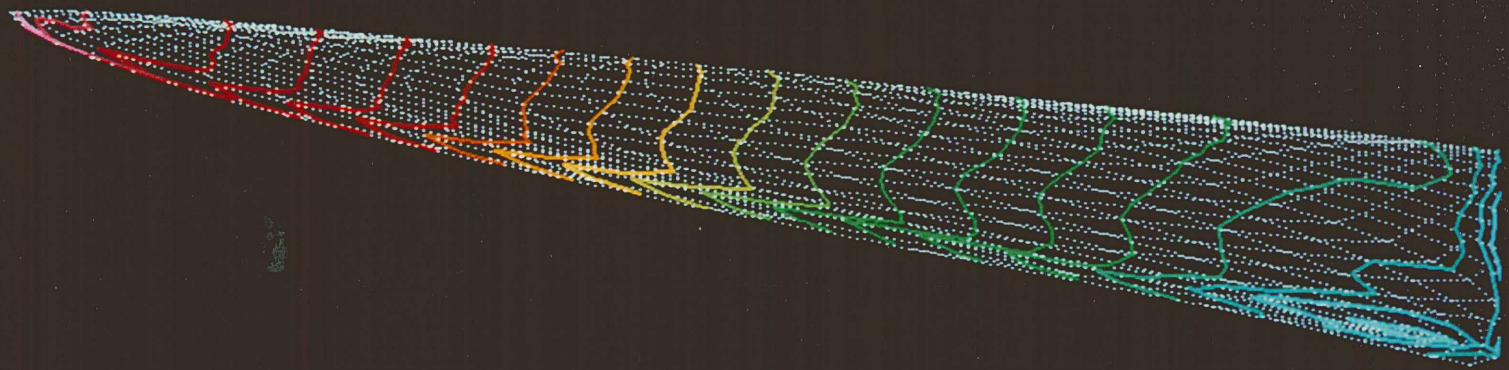
Figure 11. Symmetry Plane Contours of Pressure Differences,
 $M_\infty = 1.05$, $\alpha = 10$ deg.

PRESSURE COEFFICIENT

CONTOUR LEVELS

- 0.02100
- 0.02000
- 0.01900
- 0.01800
- 0.01700
- 0.01600
- 0.01500
- 0.01400
- 0.01300
- 0.01200
- 0.01100
- 0.01000
- 0.00900
- 0.00800
- 0.00700
- 0.00600
- 0.00500
- 0.00400
- 0.00300
- 0.00200
- 0.00100
- 0.00000
- 0.00100
- 0.00200
- 0.00300
- 0.00400

0.950 MACH
20.00 DEG ALPHA
2.00x10⁶ Re
30x31x14 GRID



25

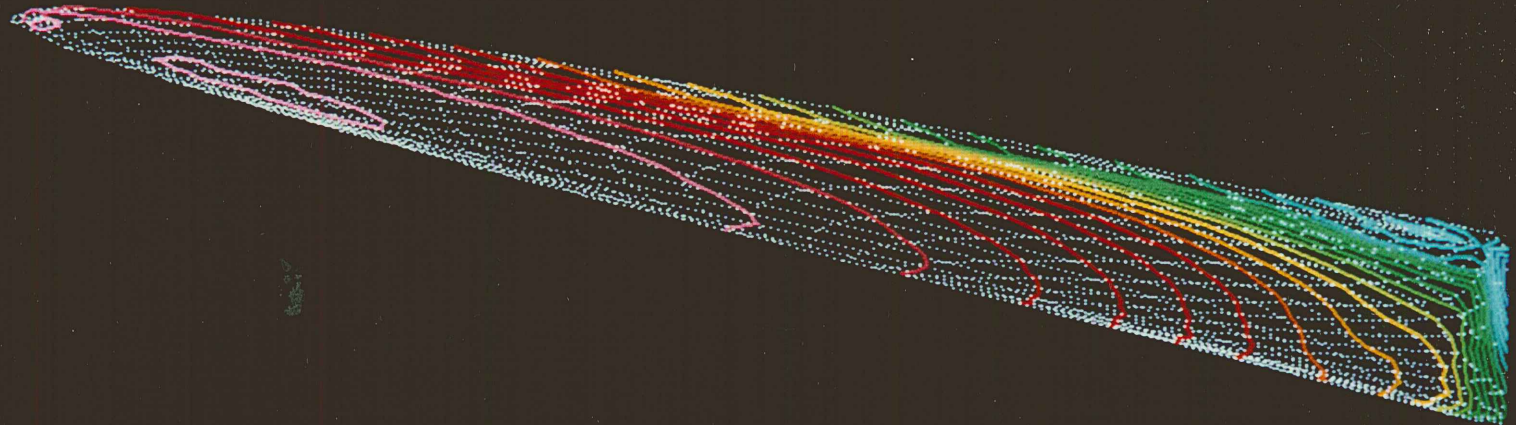
a. Top Surface
Figure 12. Distribution of Interference on Model Surface,
 $M_\infty = 0.95$, $\alpha = 20$ deg.

PRESSURE COEFFICIENT

CONTOUR LEVELS

- .02100
- .02000
- .01900
- .01800
- .01700
- .01600
- .01500
- .01400
- .01300
- .01200
- .01100
- .01000
- .00900
- .00800
- .00700
- .00600
- .00500
- .00400
- .00300
- .00200
- .00100
- 0.00000
- 0.00100
- 0.00200
- 0.00300
- 0.00400

0.950 MACH
20.00 DEG ALPHA
 2.00×10^{06} Re
30x31x14 GRID



b. Bottom Surface
Figure 12. Concluded.

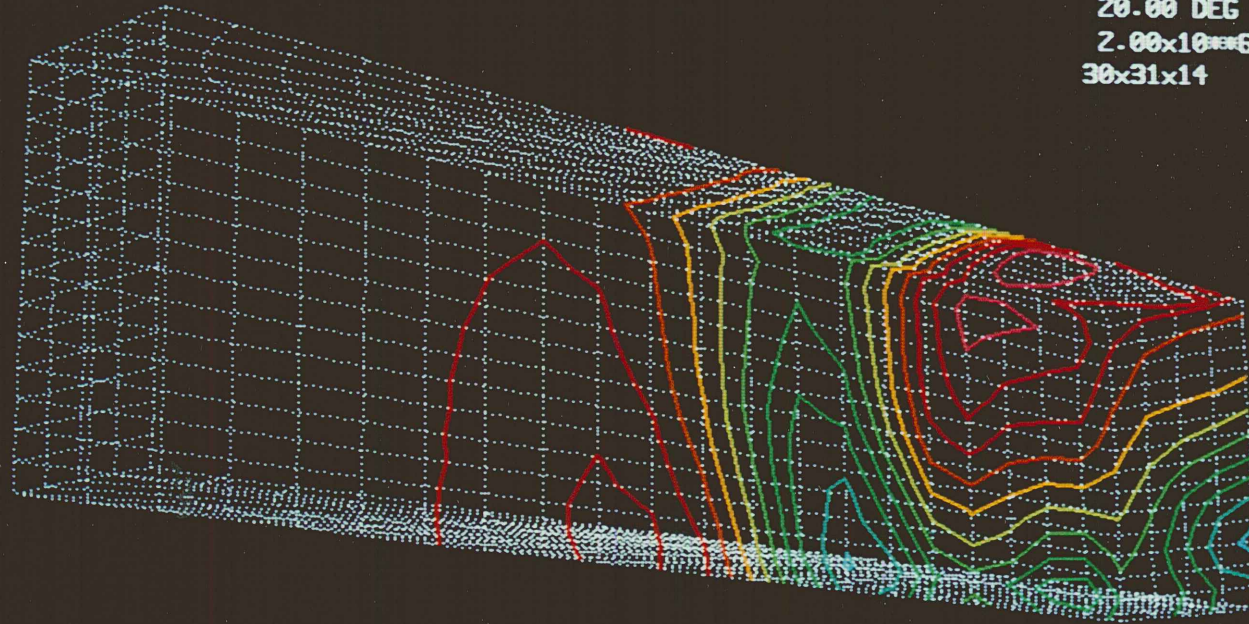
PRESSURE COEFFICIENT

CONTOUR LEVELS

- 0.02200
- 0.02000
- 0.01800
- 0.01600
- 0.01400
- 0.01200
- 0.01000
- 0.00800
- 0.00600
- 0.00400
- 0.00200
- 0.00000
- 0.00200
- 0.00400
- 0.00600
- 0.00800
- 0.01000

0.950
20.00 DEG
 2.00×10^{06}
30x31x14

MACH
ALPHA
Re
GRID



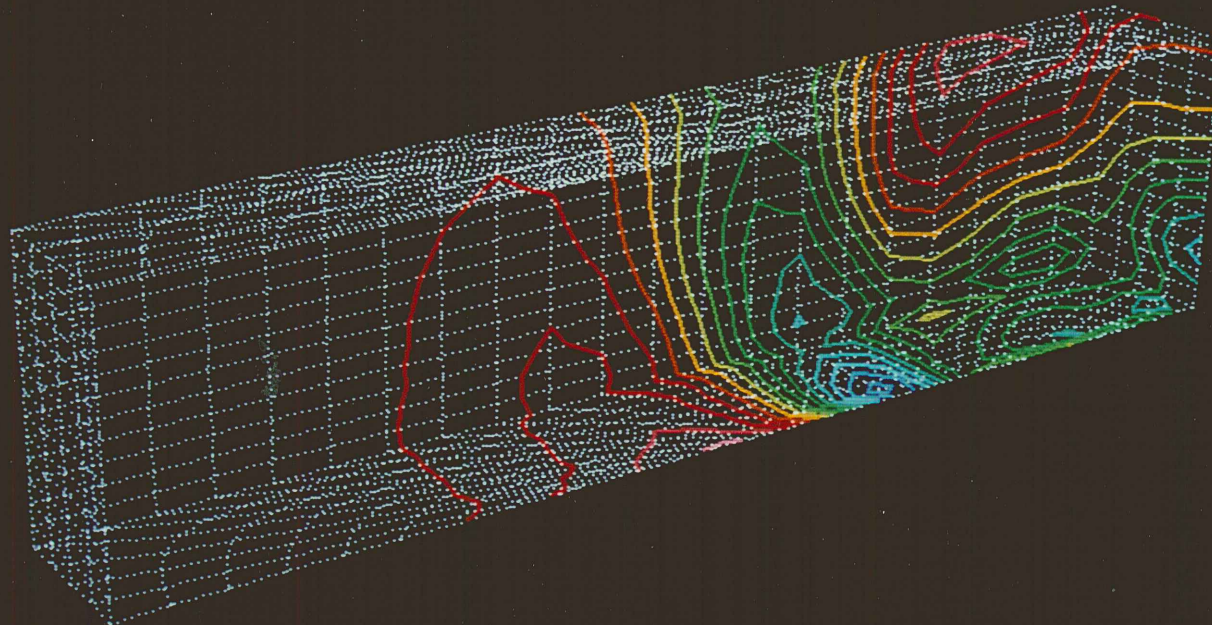
a. Top and Side Surface
Figure 13. Distribution of Interference on Tunnel Boundary,
 $M_\infty = 0.95$, $\alpha = 20$ deg

PRESSURE COEFFICIENT

CONTOUR LEVELS

-.02200
-.02000
-.01800
-.01600
-.01400
-.01200
-.01000
-.00800
-.00600
-.00400
-.00200
0.00000
0.00200
0.00400
0.00600
0.00800
0.01000

0.950 MACH
20.00 DEG ALPHA
 2.00×10^{06} Re
30x31x14 GRID



b. Bottom and Side Surface
Figure 13. Concluded.

PRESSURE COEFFICIENT

CONTOUR LEVELS

- 0.02200
- 0.02000
- 0.01800
- 0.01600
- 0.01400
- 0.01200
- 0.01000
- 0.00800
- 0.00600
- 0.00400
- 0.00200
- 0.00000
- 0.00200
- 0.00400
- 0.00600
- 0.00800
- 0.01000

0.950 MACH
20.00 DEG ALPHA
2.00x10⁶ Re
30x31x14 GRID

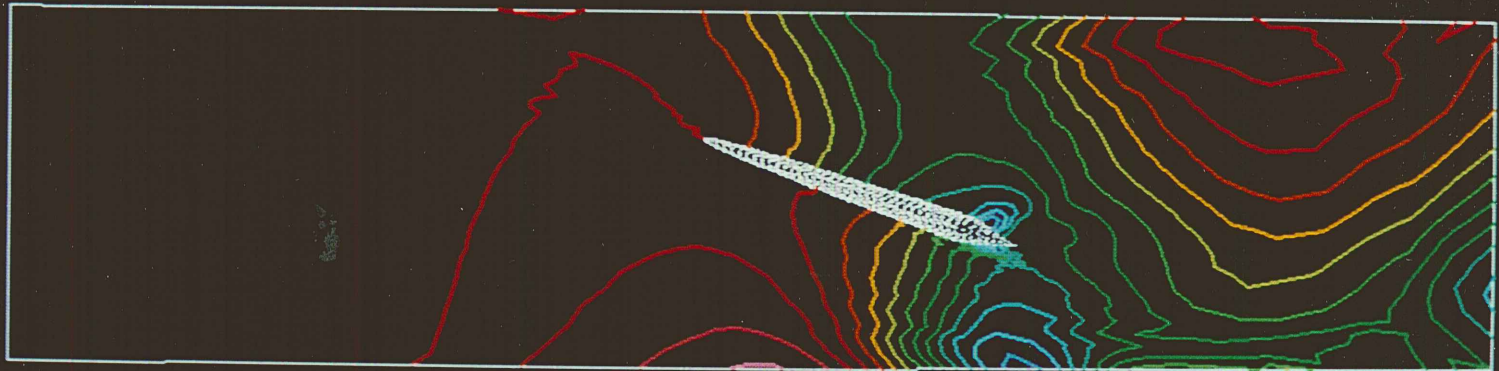


Figure 14. Symmetry Plane Contours of Pressure Differences,
 $M_\infty = 0.95$, $\alpha = 20$ deg.

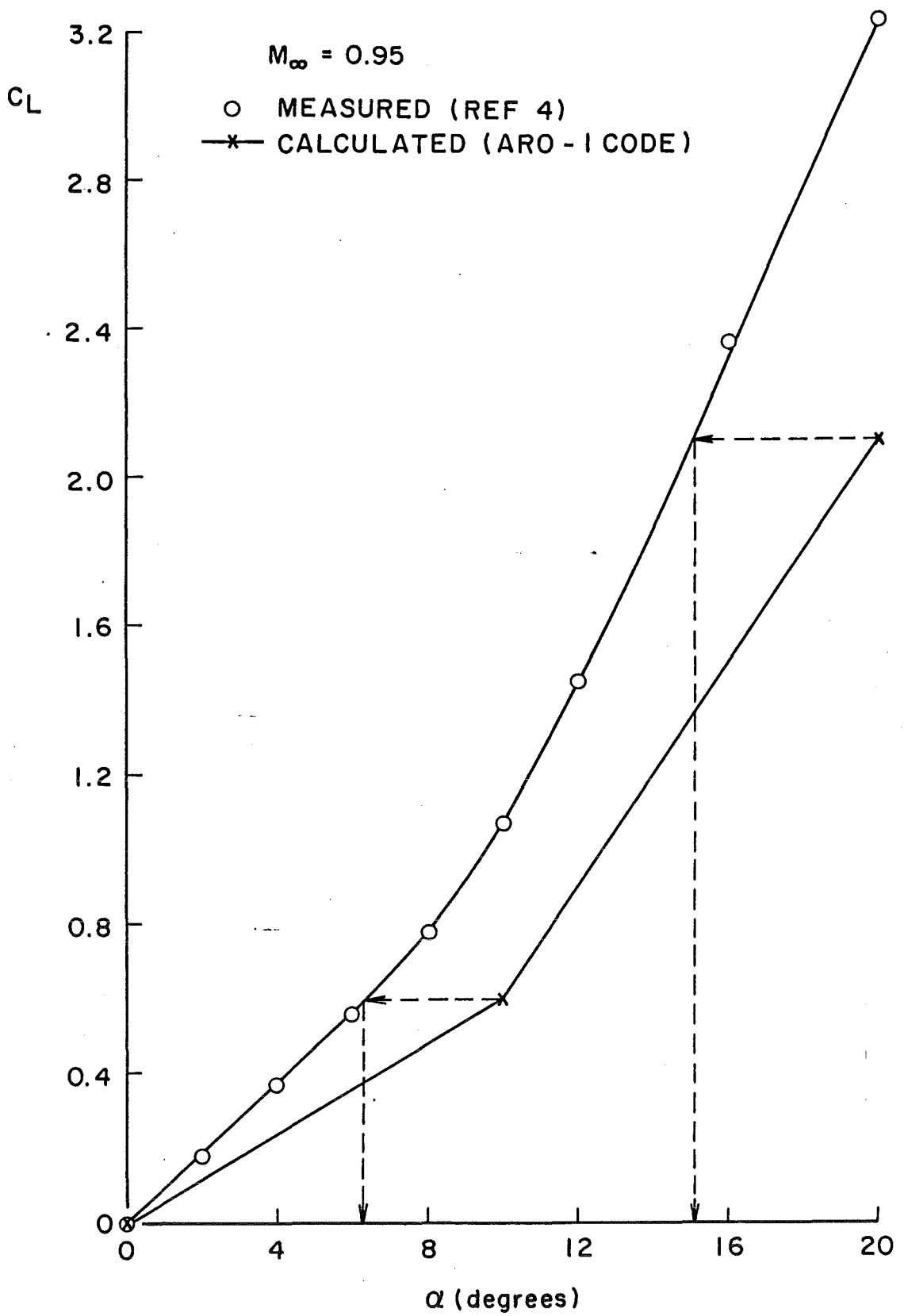
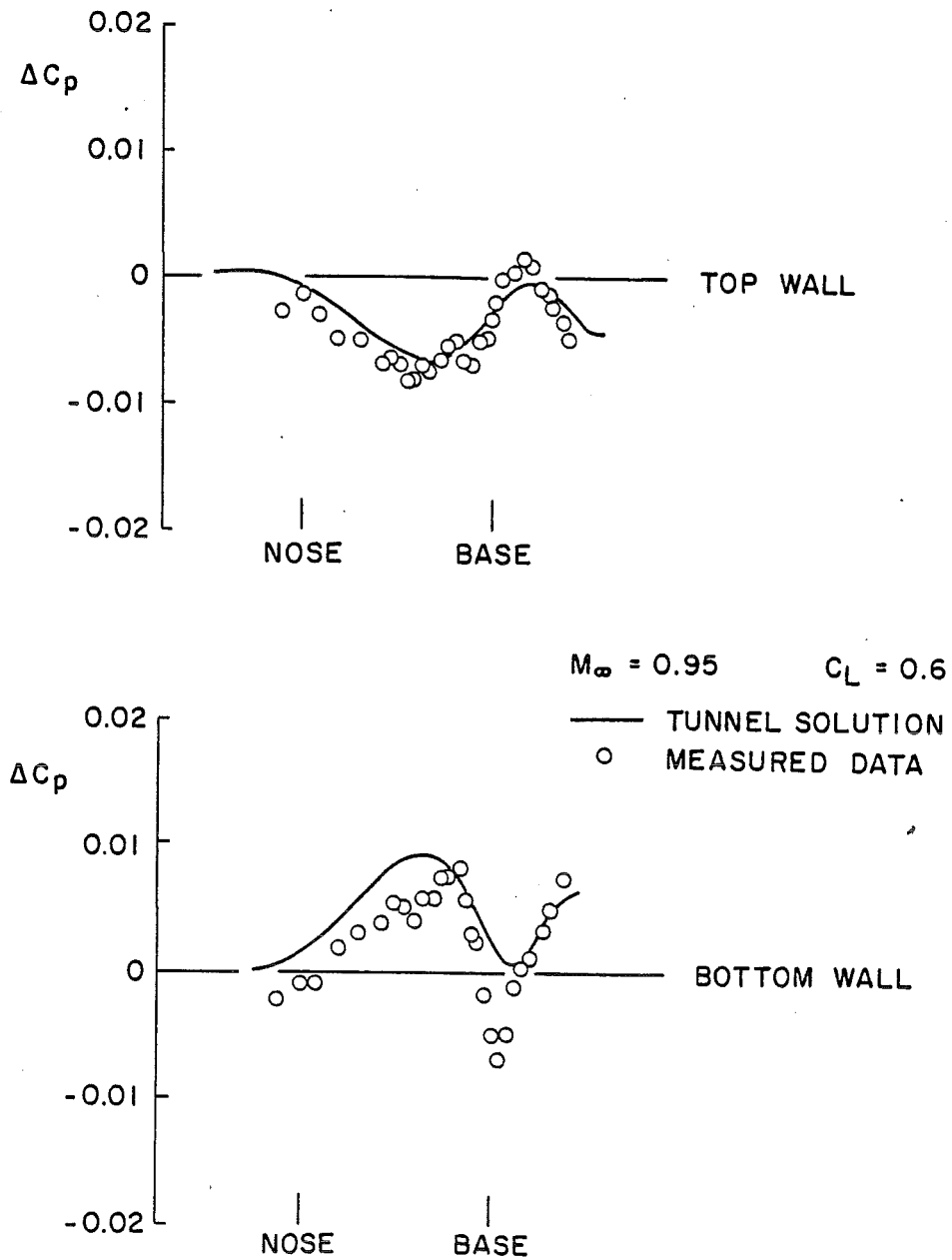
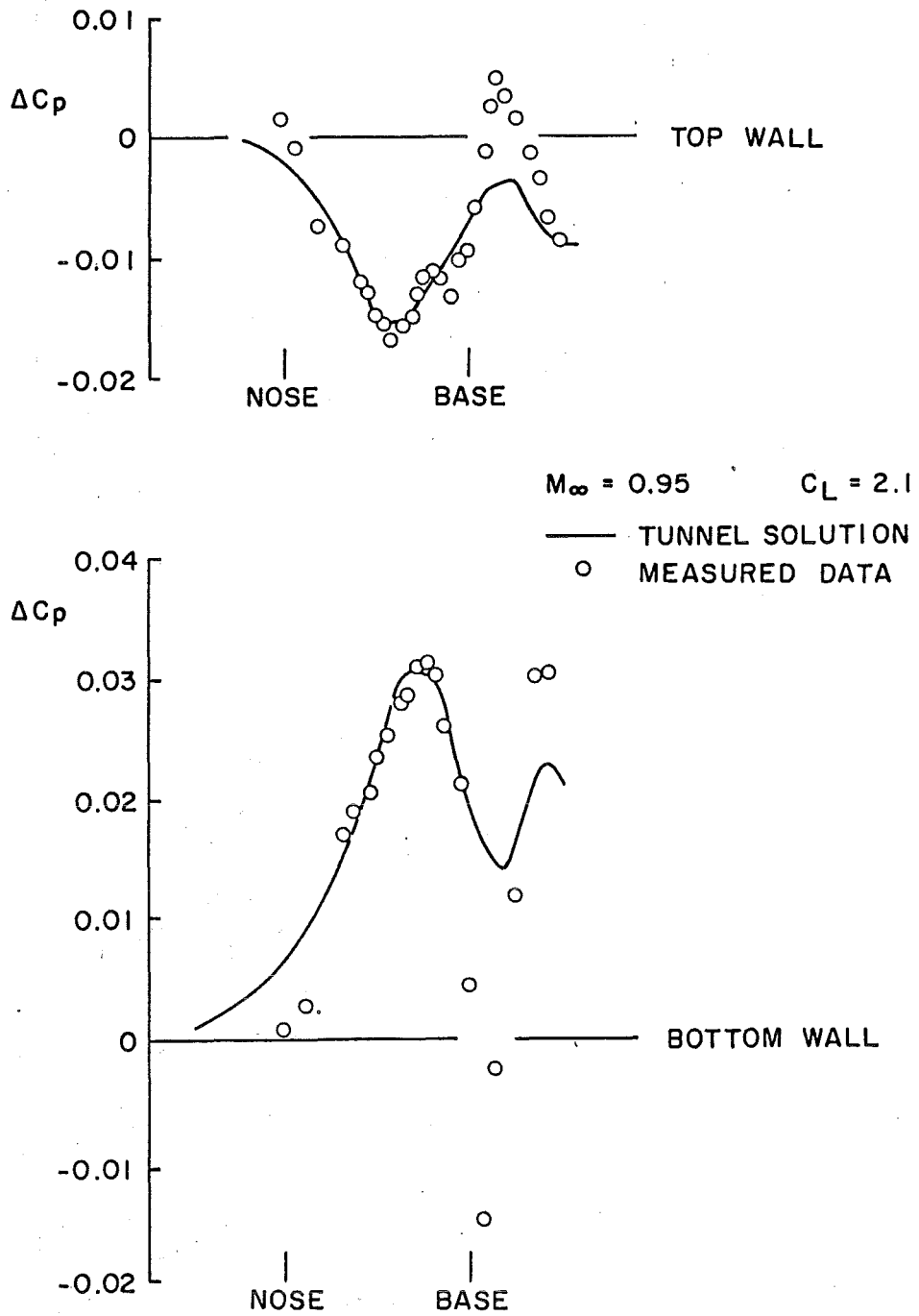


Figure 15. Computed and Measured Lift vs Angle-of-Attack in PWT-4T, $M = 0.95$



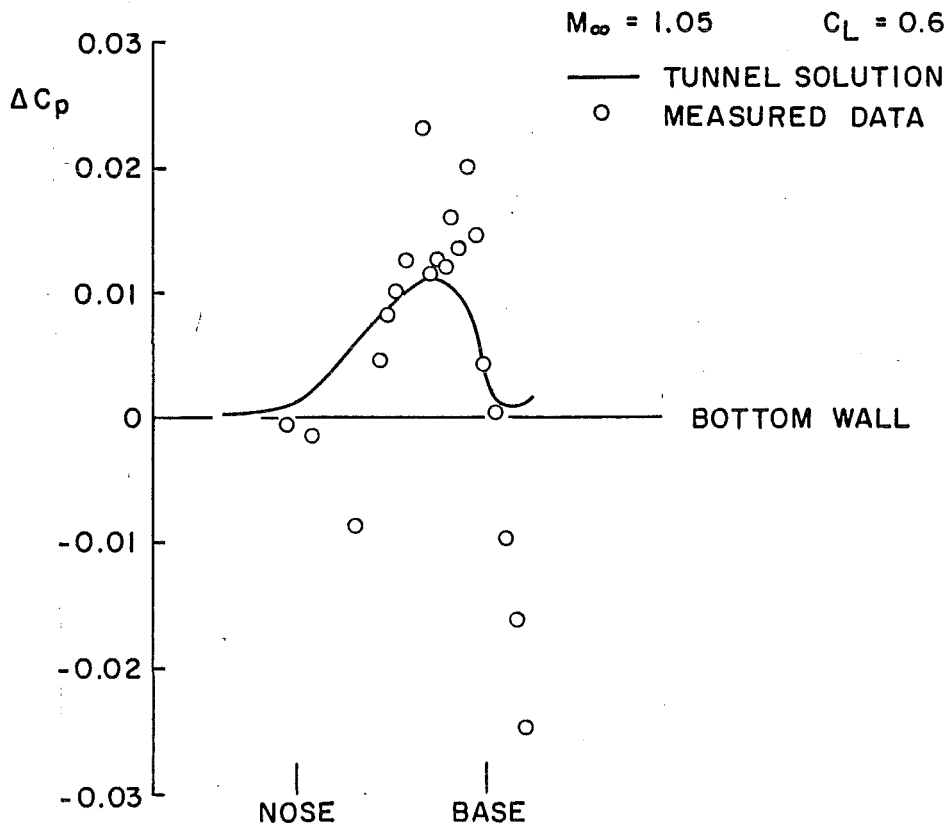
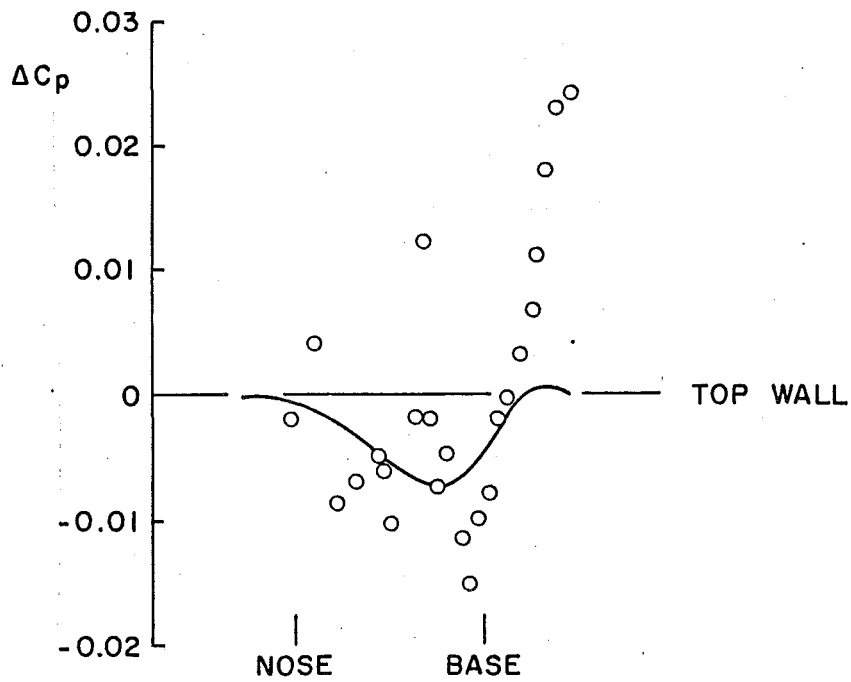
a. $M = 0.95$, $C_L = 0.6$

Figure 16. Computed and Measured Wall Static Pressure Comparisons in PWT-4T



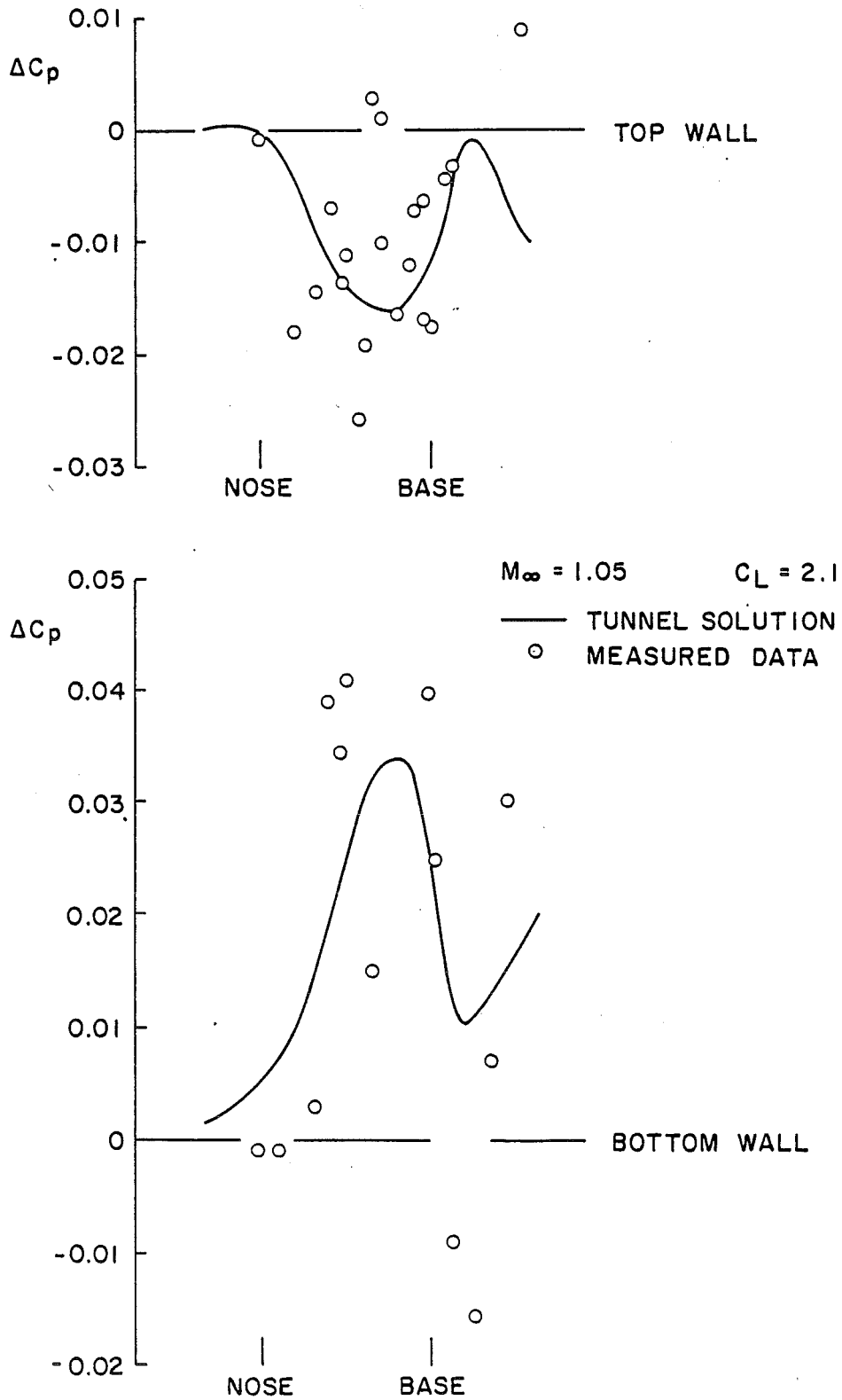
b. $M = 0.95, C_L = 2.1$

Figure 16. Continued



c. $M = 1.05, C_L = 0.6$

Figure 16. Continued



d. $M = 1.05$, $C_L = 2.1$
 Figure 16. Concluded

Table 1. Summary of Integrated Wall Interference Effects
on Model Force and Moment

$M_\infty = 0.95$		
	$C_L = 0.6$	$C_L = 2.1$
	$C_m = 0.49$	$C_m = 0.86$
ΔC_L	0.0177	0.0540
ΔC_m	0.0033	-0.0002

$M_\infty = 1.05$		
	$C_L = 0.6$	
	$C_m = 0.47$	
ΔC_L	0.0195	
ΔC_m	-0.0015	